Mineralogical Magazine, April 2017, Vol. 81(2), pp. 329–338

Steinmetzite, $Zn_2Fe^{3+}(PO_4)_2(OH)\cdot 3H_2O$, a new mineral formed from alteration of phosphophyllite at the Hagendorf Süd pegmatite, Bavaria

I. E. Grey[1,*], E. Keck[2], A. R. Kampf[3], W. G. Mumme[1], C. M. Macrae[1], R. W. Gable[4], A. M. Glenn[1] and C. J. Davidson[1]

[1] CSIRO Mineral Resources, Private Bag 10, Clayton South, Victoria 3169, Australia
[2] Algunderweg 3, D-92694 Etzenricht, Germany
[3] Mineral Sciences Department, Natural History Museum of Los Angeles County 900 Exposition Boulevard, Los Angeles, CA 90007, USA
[4] School of Chemistry, University of Melbourne, Parkville, Victoria 3010, Australia

[*Received 24 November 2015; Accepted 10 March 2016; Associate Editor: Andrew Christy*]

ABSTRACT

Steinmetzite, ideally $Zn_2Fe^{3+}(PO_4)_2(OH)\cdot 3H_2O$, is a new mineral from the Hagendorf-Süd pegmatite, Hagendorf, Oberpfalz, Bavaria, Germany. Steinmetzite was found in a highly oxidized zone of the Cornelia mine at Hagendorf-Süd. It has formed by alteration of phosphophyllite, involving oxidation of the iron and some replacement of Zn by Fe. Steinmetzite lamellae co-exist with an amorphous Fe-rich phosphate in pseudomorphed phosphophyllite crystals. The lamellae are only a few μm thick and with maximum dimension ~50 μm. The phosphophyllite pseudomorphs have a milky opaque appearance, often with a glazed yellow to orange weathering rind and with lengths ranging from sub-mm to 1 cm. Associated minerals are albite, apatite, chalcophanite, jahnsite, mitridatite, muscovite, quartz and wilhelmgümbelite. Goethite and cryptomelane are also abundant in the oxidized zone. The calculated density is 2.96 g cm^{-3}. Steinmetzite is biaxial (–) with measured refractive indices $\alpha = 1.642(2)$, $\beta = 1.659$ (calc.), $\gamma = 1.660(2)$ (white light). 2V(meas) = 27(1)°; orientation is $Y \approx \mathbf{b}$, $X \wedge \mathbf{c} \approx 27°$, with crystals flattened on {010} and elongated on [001]. Pleochroism shows shades of pale brown; $Y > X \approx Z$. Electron microprobe analyses (average of seven crystals) with Fe reported as Fe_2O_3 and with H_2O calculated from the structure gave ZnO 31.1, MnO 1.7, CaO 0.5, Fe_2O_3 21.9, Al_2O_3 0.3, P_2O_5 32.9, H_2O 14.1 wt.%, total 102.5%. The empirical formula based on 2 P and 12 O, with all iron as ferric and OH^- adjusted for charge balance is $Zn_{1.65}Fe^{3+}_{1.19}Mn^{2+}_{0.11}Ca_{0.03}Al^{3+}_{0.02}(PO_4)_2(OH)_{1.21}\cdot 2.79H_2O$. The simplified formula is $Zn_2Fe^{3+}(PO_4)_2(OH)\cdot 3H_2O$. Steinmetzite is triclinic, $P\bar{1}$, with unit-cell parameters: $a = 10.438(2)$, $b = 5.102(1)$, $c = 10.546(2)$ Å, $\alpha = 91.37(2)$, $\beta = 115.93(2)$ and $\gamma = 94.20(2)°$. $V = 502.7(3)$ Å^3, $Z = 2$. The strongest lines in the powder X-ray diffraction pattern are [d_{obs} in Å (I) (*hkl*)] 9.313(65) (100), 5.077(38) (010), 4.726(47) (002), 4.657(100) (200), 3.365 (55) ($\bar{3}02$), 3.071(54) ($1\bar{1}2$) and 2.735(48) ($\bar{3}\bar{1}2$). The structure is related to that of phosphophyllite.

Keywords: new mineral, new secondary phosphate, new phosphophyllite-related mineral, crystal structure.

Introduction

The new secondary phosphate mineral steinmetzite was discovered by EK when collecting specimens in the Cornelia mine at the Hagendorf-Süd pegmatite deposit in 1977. The phosphate-rich granite pegmatite of Hagendorf-Süd is the type locality for 16 valid minerals of which all but one are phosphates. With the closing of the mine and natural flooding in 1984, access for mineral collecting was no longer possible. Subsequently, six new secondary phosphate minerals have been

*E-mail: Ian.Grey@csiro.au
https://doi.org/10.1180/minmag.2016.080.100

characterized from studies on minerals in a collection made by EK of samples he collected during the mine operation. These are: nordgauite, $MnAl_2(PO_4)_2(F,OH)_2 \cdot 5H_2O$ (Birch *et al*., 2011); whiteite-(CaMnMn), $CaMnMn_2Al_2(PO_4)_4(OH)_2 \cdot 8H_2O$ (Yakovenchuk *et al*., 2012); flurlite, $Zn_3Mn^{2+}Fe^{3+}(PO_4)_3(OH)_2 \cdot 9H_2O$ (Grey *et al*., 2015*b*); kummerite, $Mn^{2+}Fe^{3+}Al(PO_4)_2(OH)_2 \cdot 8H_2O$ (Grey *et al*., 2016); kayrobertsonite, $MnAl_2(PO_4)_2(OH)_2 \cdot 6H_2O$ (Mills *et al*., 2016); wilhelmgümbelite, $[ZnFe^{2+}Fe^{3+}_3(PO_4)_3(OH)_4(H_2O)_5] \cdot 2H_2O$ (Grey *et al*., 2017).

The new mineral, steinmetzite, is another example of a secondary phosphate obtained from hand specimens in the Keck collection. The name and data for steinmetzite have been approved by the International Mineralogical Association Commission on New Minerals, Nomenclature and Classification (IMA2015-081, Grey *et al*., 2015*a*). The mineral is named for Dr. Hermann Steinmetz, born in 1879 in Regensberg and died in 1964. He was the Curator of Mineralogy at the Munich museum Sammlung des Bayerischen Staates, from 1923 to 1928 and was Professor of Mineralogy and Geology at the Technische Hochschule, Munich from 1928 to 1950. After WW2, Dr. Steinmetz was responsible for the re-establishment of the destroyed Institute of Mineralogy and Geology at Munich. Dr. Steinmetz was the first to publish the correct analysis and composition of phosphophyllite (Laubmann and Steinmetz, 1920; Steinmetz, 1926). The holotype specimen used for all measurements is housed in the mineralogical collections at Museum Victoria, registration number M53510.

Occurrence, mineral assemblage and paragenesis

Steinmetzite occurs in phosphophyllite pseudomorphed crystals in a highly oxidized zone of the Cornelia mine open cut at the Hagendorf-Süd pegmatite, Hagendorf, Oberpfalz, Bavaria, Germany (49°39′1″N, 12°27′35″E). It was identified by its unique powder X-ray diffraction (XRD) pattern, shown in Fig. 1, in only a few specimens at depths of 60 to 67 metres in the mine. The new mineral occurs as lamellae within altered phosphophyllite crystals, where it is intergrown with an X-ray amorphous Fe-rich phosphate. The lamellae are only a few μm thick and with a maximum dimension of the order of 50 μm. The phosphophyllite pseudomorphs are associated closely with wilhelmgümbelite, $[ZnFe^{2+}Fe^{3+}_3(PO_4)_3(OH)_4(H_2O)_5] \cdot 2H_2O$, a low-Mn variety of oxidized schoonerite (Grey *et al*., 2017). Other associated minerals that have been identified by XRD are albite, apatite, chalcophanite, jahnsite, mitridatite, muscovite and quartz. Goethite and

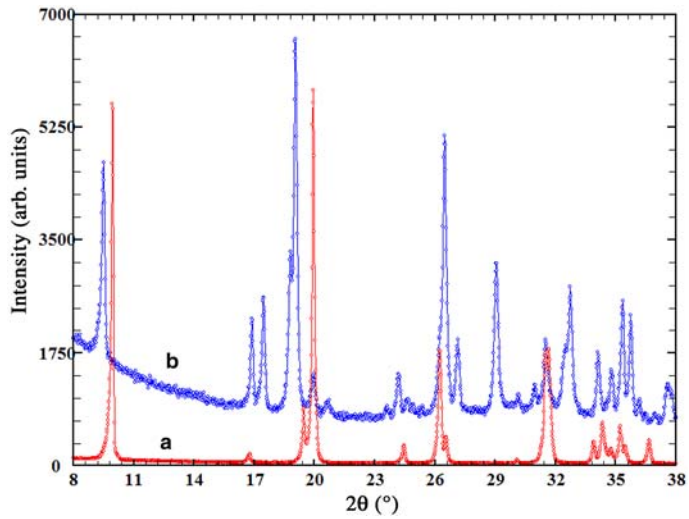

FIG. 1. Comparison of powder XRD patterns (CuKα) for (*a*) fresh phosphophyllite and (*b*) altered phosphophyllite, for which all the Bragg peaks correspond to steinmetzite. The peaks for phosphophyllite have been scaled so that the strongest peaks in the two minerals have the same intensity.

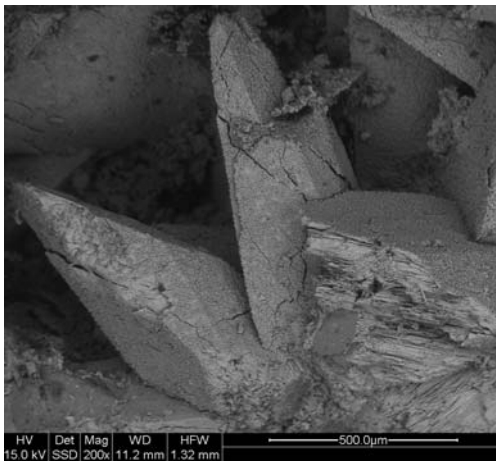

FIG. 2. Back-scattered scanning electron image of altered phosphophyllite crystals, composed of intergrown steinmetzite and an amorphous Fe-rich phosphate. The crystal at the bottom right has been broken, displaying a lamella type internal structure.

cryptomelane are also abundant in the oxidized zone.

Steinmetzite is a secondary phosphate mineral that has formed by oxidation of Fe^{2+} in phosphophyllite. The alteration of phosphophyllite also involves extensive replacement of Zn by Fe, producing an amorphous Fe-rich phosphate that coexists with steinmetzite.

Physical and optical properties

In contrast to the pale green transparent crystals of fresh phosphophyllite, the pseudomorphed phosphophyllite crystals at Hagendorf Süd have a milky opaque appearance, often with a glazed yellow to orange weathering rind. Mücke (1981) has reported previously that phosphophyllite at Hagendorf frequently has a "muddied and opaque appearance" and displays "a reproducible but as yet an unidentified X-ray diagram". The crystals have the "stretched, pointed" morphology, described by Forster *et al*. (1967), with lengths ranging from sub-mm to 1 cm. Typical crystals are shown in Fig. 2. The interior of the crystals are white to cream in colour and at low magnifications appear to be fibrous. At higher magnifications, the 'fibres' are seen to be thin platelets viewed edge-on as illustrated by the crystal in the lower right of Fig. 2. Powder XRD patterns obtained on crushed phosphophyllite pseudomorphs show relatively sharp peaks due to steinmetzite superimposed on broad humps from an X-ray amorphous phase, shown in Fig. 3. From a comparison of the powder XRD patterns for fresh and altered phosphophyllite, the amount of the amorphous phase is estimated to be 80 to >90 wt.%. The amorphous phase is readily distinguished optically from the biaxial crystals of steinmetzite by being optically isotropic. The two phases are also easily distinguished in a scanning electron microscope using back-scattered electron (BSE) images and energy-dispersive analysis

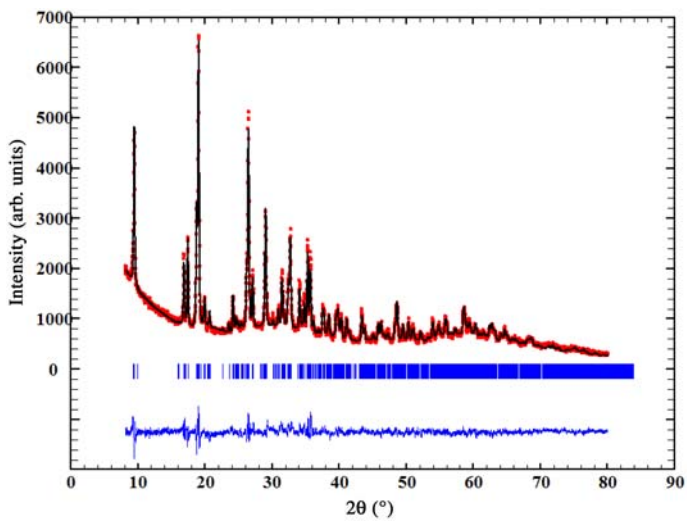

FIG. 3. Rietveld fit to steinmetzite powder XRD data (Cu$K\alpha$). Black line is calculated, red dots are observed and blue line is difference. Blue tick marks indicate Bragg reflections.

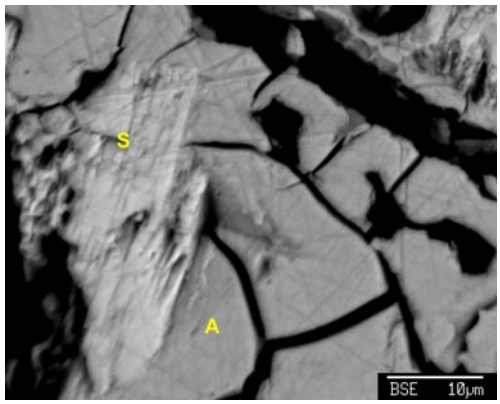

FIG. 4. Back-scattered electron image of steinmetzite (S) and amorphous Fe-rich phosphate (A) in pseudomorphed phosphophyllite.

(EDA). Steinmetzite has a high Zn content and appears brighter than the amorphous Fe-rich phase. A typical BSE image is shown in Fig. 4. A feature of the pseudomorphed phosphophyllite is the extensive internal cracking and fracturing, on a scale of ~10 μm, shown in Fig. 4. Cleavage of steinmetzite is good parallel to {010}. The crystals are flattened on {010} and elongated on [001]. Steinmetzite is non-fluorescent, has a white streak, is brittle and has an uneven fracture. The density could not be measured because of the fine-scale intergrowth with the amorphous phase. The calculated density is 2.96 g cm^{-3}.

Steinmetzite is biaxial (–) with measured indices of refraction $\alpha = 1.642(2)$, $\beta = 1.659$ (calc.), $\gamma = 1.660(2)$ (white light). 2V(meas) = 27(1)° based on extinction data analysed using *EXCALIBR* (Gunter *et al*., 2004). The unfavourable orientation of *Y* approximately perpendicular to the thin parallel plates prevented the measurement of β; consequently it was calculated from α, γ and 2V. The orientation is $Y \approx \mathbf{b}$, $X \wedge \mathbf{c} \approx 27°$. Pleochroism shows shades of pale brown; $Y > X \approx Z$. The Gladstone-Dale compatibility index (Mandarino, 1981) calculated using the above optical properties with the empirical formula and calculated density is 0.021, which is classed as excellent.

Chemical composition

Crystals of steinmetzite were analysed using wavelength dispersive spectrometry on a JEOL JXA 8500F Hyperprobe operated at an accelerating voltage of 12 kV and a beam current of 4 nA. The beam was typically defocused to 2 μm. Water was not analysed directly because of the fine-scale mixing with an amorphous Fe-rich phosphate. It was calculated from the structure, with 4 ($H_2O + OH^-$) per formula unit. Analytical results from analysis of seven crystals (7 points) are given in Table 1.

The empirical formula based on the relationship to phosphophyllite and structure refinement, based on 2 P and 12 O, with all iron as ferric and OH^- adjusted for charge balance is $Zn_{1.65}Fe^{3+}_{1.19}Mn^{2+}_{0.11}Ca_{0.03}Al^{3+}_{0.02}(PO_4)_2(OH)_{1.21}\cdot 2.79H_2O$. The simplified formula is $Zn_2Fe^{3+}(PO_4)_2(OH)\cdot 3H_2O$.

Crystallography

Powder X-ray diffraction

Powder XRD data were collected using a Philips diffractometer, graphite monochromator and Cu*K*α radiation. The atomic coordinates from the single-crystal refinement were employed in a Rietveld fitting of the powder pattern using *FULLPROF* (Rodriguez-Carvajal, 1990). The good fit to the powder pattern, shown in Fig. 3, ensured that there were no ambiguities in the indexing of the pattern,

TABLE 1. Analytical data (wt.%) for steinmetzite.

Constituent	Mean	Range	Standard deviation	Probe standard
ZnO	31.1	25.6–34.6	2.9	phosphophyllite
MnO	1.74	1.52–2.01	0.15	rhodonite
CaO	0.45	0.25–0.67	0.18	fluorite
Fe_2O_3	21.9	19.6–25.2	2.3	hematite
Al_2O_3	0.26	0.13–0.48	0.13	berlinite
P_2O_5	32.9	31.7–34.9	1.0	berlinite
H_2O*	14.1			
Total	102.45			

*based on structure refinement.

TABLE 2. Powder diffraction data (d in Å) for steinmetzite.

I_{meas}	I_{calc}	d_{meas}	d_{calc}	h	k	l
65	52	9.313	9.335	1	0	0
28	21	5.251	5.251	$\bar{1}$	0	2
38	28	5.077	5.080	0	1	0
47	34	4.726	4.725	0	0	2
100	30	4.657	4.668	2	0	0
	70		4.651	1	$\bar{1}$	0
12	11	4.445	4.442	$\bar{2}$	0	2
8	5	4.296	4.294	1	1	0
5	4	3.766	3.769	$\bar{2}$	1	1
18	13	3.679	3.678	$\bar{1}$	$\bar{1}$	2
5	3	3.614	3.612	2	$\bar{1}$	0
5	4	3.572	3.570	0	$\bar{1}$	2
20	15	3.397	3.340	$\bar{2}$	1	2
55	35	3.365	3.370	$\bar{3}$	0	2
	42		3.359	0	1	2
22	14	3.284	3.285	2	1	0
54	43	3.071	3.072	1	$\bar{1}$	2
9	7	2.886	2.888	$\bar{3}$	1	2
19	18	2.838	2.839	1	1	2
17	17	2.754	2.753	0	$\bar{1}$	3
48	31	2.735	2.734	$\bar{3}$	$\bar{1}$	2
19	14	2.626	2.626	$\bar{2}$	0	4
14	10	2.577	2.577	$\bar{1}$	0	4
39	28	2.539	2.540	0	2	0
31	23	2.511	2.512	1	$\bar{2}$	0
6	4	2.482	2.481	$\bar{3}$	0	4
8	9	2.391	2.394	1	2	0
10	8	2.381	2.382	$\bar{4}$	1	2
8	5	2.340	2.341	2	1	2
6	5	2.333	2.334	4	0	0
8	5	2.276	2.279	1	1	3
	4		2.274	$\bar{1}$	2	2
11	11	2.261	2.262	$\bar{1}$	1	4
6	4	2.234	2.237	$\bar{2}$	2	2
	4		2.232	1	2	1
5	4	2.194	2.194	0	$\bar{1}$	4
	3		2.192	3	0	2
6	5	2.084	2.086	3	$\bar{1}$	2
	5		2.082	1	0	4
6	4	2.066	2.066	3	$\bar{2}$	0
4	2	2.012	2.011	$\bar{4}$	$\bar{1}$	4
8	6	1.978	1.978	$\bar{5}$	1	2
8	8	1.962	1.963	2	$\bar{2}$	2
2	2	1.922	1.923	3	$\bar{2}$	1
5	5	1.882	1.882	3	2	0
20	17	1.872	1.872	$\bar{5}$	$\bar{1}$	2
8	6	1.840	1.839	$\bar{2}$	$\bar{2}$	4
9	7	1.812	1.813	$\bar{2}$	2	4
5	4	1.790	1.791	2	2	2
7	3	1.700	1.700	$\bar{4}$	2	4
	5		1.698	$\bar{4}$	0	6
4	3	1.672	1.672	$\bar{6}$	1	2
3	3	1.643	1.645	$\bar{4}$	$\bar{2}$	4
	3		1.642	2	$\bar{3}$	0
5	4	1.576	1.576	3	0	4
	4		1.575	0	0	6
5	4	1.572	1.572	$\bar{1}$	1	6
	3		1.572	$\bar{6}$	$\bar{1}$	4
6	5	1.556	1.556	6	0	0

and allowed the assignment of only the strongest reflection indices where overlapping of reflections occurred. The indexed powder data is reported in Table 2. Triclinic unit-cell parameters, refined from the powder data are: $a = 10.4319(7)$, $b = 5.1041(3)$, $c = 10.5330(6)$ Å, $\alpha = 91.222(4)$, $\beta = 115.984(4)$, $\gamma = 94.352(4)°$, $V = 501.76(5)$ Å^3.

Single-crystal studies

Phosphophyllite pseudomorphs were examined initially using the precession method. They gave single-crystal patterns, albeit with a large mosaic spread of the spots and streaking along [100]*. The large mosaicity can be understood in terms of the crystals being composed of small lamellae of steinmetzite, separated by regions of the amorphous Fe-rich phosphate, with the extensive fracturing of the amorphous phase causing misalignment of the steinmetzite crystals. A phosphophyllite crystal pseudomorph was chosen in which the mosaic spread was less severe and a single-crystal data set was collected on an Oxford Diffraction SuperNova diffractometer using Cu$K\alpha$ radiation. The refined single-crystal unit-cell parameters for steinmetzite are: $a = 10.438(2)$, $b = 5.102(1)$, $c = 10.546(2)$ Å, $\alpha = 91.37(2)$, $\beta = 115.93(2)$ and $\gamma = 94.20(2)°$. $V = 502.7(3)$ Å^3.

The structure of steinmetzite was solved in the triclinic space group $P\bar{1}$ using the spin flipping algorithm, *Superflip*, implemented in *JANA2006* (Petříček *et al*., 2014). All non-hydrogen atoms were present in the structure solution, which refined to $wR_{obs} = 0.128$ for 492 observed reflections with $I > 2\sigma(I)$, using isotropic displacement parameters. The refinement took account of there being less than 2 Zn in the empirical formula by refining the occupancies of Fe+Zn (where Fe accounts also for

TABLE 3. Data collection and refinement details for steinmetzite.

Ideal formula	$Zn_2Fe^{3+}(PO_4)_2(OH)\cdot 3H_2O$
Formula weight	447.6
Temperature	293(2) K
Wavelength	1.5418 Å
Crystal system	Triclinic
Space group	$P\bar{1}$
Unit-cell dimensions	$a = 10.438(2)$ Å $\quad \alpha = 91.37(2)°$
	$b = 5.102(1)$ Å $\quad \beta = 115.93(2)°$
	$c = 10.546(2)$ Å $\quad \gamma = 94.20(2)°$
Volume	502.7(3) Å^3
Z	2
Density (calculated)	2.957 g cm^{-3}
Absorption coefficient	20.68 mm^{-1}
F(000)	424
Crystal size (mm)	0.37 × 0.31 × 0.23
Theta range for data collection	4.67 to 55.37°
Index ranges	$-11 \leq h \leq 13$, $-6 \leq k \leq 6$, $-13 \leq l \leq 9$
Reflections collected	3579
Independent reflections	1519 [R(int) = 0.159]
Reflections with $I > 2\sigma(I)$	492
Completeness	98%
Refinement method	Full-matrix least-squares on F^2
Data/restraints/parameters	1519 / 0 / 70
Goodness-of-fit on F^2	1.05
Final R indices [$I > 2\sigma(I)$]	$R_{obs} = 0.128$, $wR_{obs} = 0.128$
R index (all data)	$wR_{all} = 0.176$
Largest diff. peak and hole	0.97 and –0.99 e.Å^{-3}

TABLE 4. Refined coordinates, isotropic displacement parameters and calculated bond-valence sums (BVS) for steinmetzite.

Atom	x	y	z	U_{iso} (Å^2)	BVS
Zn1*	0.0121(3)	0.7019(5)	0.6529(3)	0.046(1)	2.09(5)
Zn2*	0.0101(3)	0.2045(5)	0.8562(3)	0.045(1)	2.08(5)
Fe1	0.5	0	0.5	0.051(1)	2.67(6)
Fe2	0.5	0	0	0.055(1)	3.10(7)
P1	0.8247(5)	0.1749(9)	0.5351(6)	0.044(1)	4.9(1)
P2	0.1882(6)	0.750(1)	0.9895(6)	0.046(1)	5.1(1)
O1	0.844(2)	–0.116(3)	0.551(2)	0.059(4)	1.93(7)
O2	0.944(2)	0.341(3)	0.668(2)	0.059(4)	2.19(6)
O3	0.671(2)	0.220(3)	0.523(2)	0.059(4)	1.72(8)
O4	0.832(2)	0.286(3)	0.400(2)	0.050(3)	1.63(7)
O5	0.345(2)	0.850(3)	1.030(2)	0.056(4)	1.97(8)
O6	0.148(1)	0.860(2)	1.103(1)	0.045(3)	1.86(7)
O7	0.167(1)	0.456(3)	0.971(2)	0.047(3)	2.03(6)
O8	0.092(2)	0.877(3)	0.840(2)	0.054(3)	2.10(6)
O9 (H_2O)	0.438(2)	0.762(3)	0.818(2)	0.055(3)	0.45(2)
O10 (H_2O)	0.604(2)	0.817(4)	0.685(2)	0.065(4)	0.39(2)
O11 (H_2O)	0.454(2)	0.311(3)	0.598(2)	0.055(3)	0.40(2)
O12 (H_2O)	0.381(2)	0.285(3)	0.887(2)	0.053(3)	0.47(2)

*Refined site occupancies: Zn1 = 0.8(1)Zn + 0.2Fe, Zn2 = 0.8(1)Zn + 0.2Fe.

TABLE 5. Selected bond distances (Å) in steinmetzite.

Zn1–O1	1.93(2)	Zn2–O2	1.96(2)
Zn1–O2	1.96(2)	Zn2–O6	1.88(2)
Zn1–O4	1.94(2)	Zn2–O7	1.92(1)
Zn1–O8	1.94(2)	Zn2–O8	1.97(2)
Av.	<1.94>	Av.	<1.93>
Fe1–O3	1.95(2)	Fe2–O5	1.89(2)
Fe1–O3	1.95(2)	Fe2–O5	1.89(2)
Fe1–O10	2.06(2)	Fe2–O9	2.07(2)
Fe1–O10	2.06(2)	Fe2–O9	2.07(2)
Fe1–O11	2.07(2)	Fe2–O12	2.03(2)
Fe1–O11	2.07(2)	Fe2–O12	2.03(2)
Av.	<2.03>	Av.	<2.00>
P1–O1	1.51(2)	P2–O5	1.54(2)
P1–O2	1.58(2)	P2–O6	1.54(2)
P1–O3	1.59(2)	P2–O7	1.49(2)
P1–O4	1.57(2)	P2–O8	1.63(2)
Av.	<1.56>	Av.	<1.55>

Mn) in sites Zn1 and Zn2. The refined occupancies, 0.8(1)Zn+0.2Fe in both sites, is consistent with the empirical formula containing 1.65Zn per formula unit. Further details of the data collection and refinement are given in Table 3. Although the agreement factor is high (due to large reflection mosaicity, see above) the refinement worked well, with sensible (albeit poor) thermal parameters for all atoms and with calculated average bond lengths in the expected normal ranges for the metal atoms. Further support for the correctness of the model is that it gave a good fit to the powder diffraction pattern. The Rietveld profile fit is shown in Fig. 3, for which R_{wp} = 5.5%, R_{Bragg} = 8.5%. This is consistent with the relatively poor single-crystal refinement being due to the diffraction quality of the crystal pseudomorph rather than a problem with the structural model.

The refined atomic coordinates, isotropic displacement parameters and bond valences (calculated in *JANA2006*) from the single-crystal refinement are reported in Table 4. The bond valence for site Fe2 corresponds to Fe^{3+}, while that for site Fe1 (2.67(6)) corresponds to predominantly Fe^{3+}. In the empirical formula, all iron has been assigned as Fe^{3+}, giving a Gladstone-Dale index of 0.021 (Excellent). The bond valences for O9 to O12 are all less than 0.5, corresponding to water molecules. Selected bond distances in steinmetzite are given in Table 5.

Discussion

The structure of steinmetzite is composed of (100) layers of corner-connected ZnO_4 and PO_4 tetrahedra, shown in Fig. 5. These layers have the same topology as the layers in the structure of phosphophyllite (Hill, 1977). The layers are interconnected via *trans*-connected $Fe^{3+}O_2(H_2O,OH)_4$ octahedra as shown in Fig. 6. The location of the interlayer octahedra are quite different in steinmetzite and phosphophyllite, as illustrated by a comparison of the [001] projections of the two structures in Fig. 7. In steinmetzite, successive octahedra along [001] are at the same height along [010], so the [001] projection shows ribbons of octahedra separated by

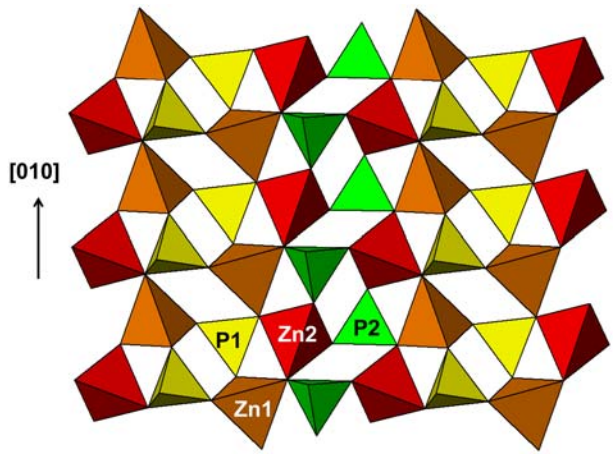

FIG. 5. {100} tetrahedral layer in steinmetzite.

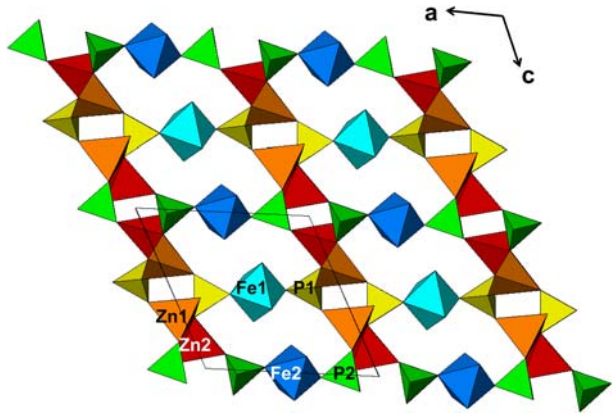

FIG. 6. [010] projection of the structure of steinmetzite

empty channels along [010]. In phosphophyllite, successive octahedra along [001] are displaced by 0.5*b*, so there are no [001] channels in phosphophyllite. The different interlayer connection pattern in steinmetzite is associated with a lowering of the symmetry from monoclinic to triclinic.

Steinmetzite can be considered crystal chemically as an oxidized form of phosphophyllite. Separating the compositions of the tetrahedral layers and the interlayer octahedra gives for phosphophyllite $[Zn_2(PO_3)_2]^{2+}[Fe^{2+}O_2(H_2O)_4]^{2-}$, whereas in steinmetzite the octahedra are occupied by Fe^{3+} and charge balance requires the octahedral composition to be $[Fe^{3+}O_2(H_2O)_3(OH)]^{2-}$. The similar values of the bond valences for the oxygen atoms of the water molecules O9 to O12, suggests that the OH^- is distributed over the four water molecule sites. An analogous situation occurs in the laueite-group minerals (Mills and Grey, 2015), which are based on heteropolyhedral layers separated by *trans*-connected $MO_2(H_2O)_4$ octahedra. Sigloite, $Fe^{3+}Al_2(PO_4)_2(OH)_3(H_2O)_7$, with $Fe^{3+}O_2(H_2O)_3(OH)$ octahedra, is the oxidized equivalent of paravauxite, $Fe^{2+}Al_2(PO_4)_2(OH)_2(H_2O)_8$, with $Fe^{2+}O_2(H_2O)_4$ octahedra (Hawthorne, 1988).

There are similarities but also important differences between steinmetzite and phosphophyllite. Comparative data for the two minerals are given in Table 6. Phosphophyllite has monoclinic symmetry, whereas steinmetzite is triclinic. Despite steinmetzite having the smaller cation Fe^{3+} replacing Fe^{2+} in phosphophyllite, the unit cell for steinmetzite is larger than for phosphophyllite. This is attributed predominantly to the different interlayer

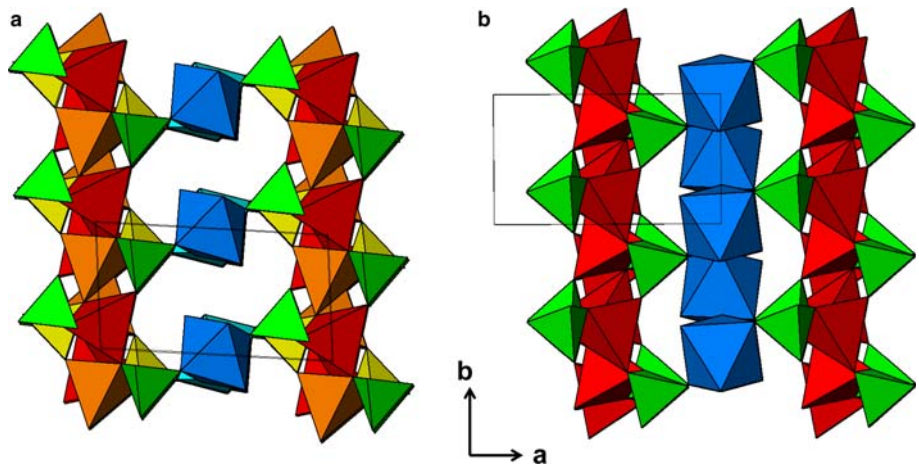

FIG. 7. [001] projections for (*a*) steinmetzite and (*b*) phosphophyllite, showing different locations of interlayer octahedra.

TABLE 6. Comparison of steinmetzite and phosphophyllite.

	Steinmetzite	Phosphophyllite
Formula (ideal)	$Zn_2Fe^{3+}(PO_4)_2(OH)\cdot 3H_2O$	$Zn_2Fe^{2+}(PO_4)_2\cdot 4H_2O$
Symmetry	Triclinic, $P\bar{1}$	Monoclinic $P2_1/c$
Cell	$a = 10.438(2)$ Å $b = 5.102(1)$ Å $c = 10.546(2)$ Å $\alpha = 91.37(2)°$ $\beta = 115.93(2)°$ $\gamma = 94.20(2)°$ $V = 502.7(3)$ Å^3	$a = 10.378(3)$ Å $b = 5.084(1)$ Å $c = 10.553(3)$ Å $\beta = 121.14(2)°$ $V = 475.7$ Å^3
Z	2	2
Strongest powder pattern lines	9.313, 65, (100) 4.726, 47, (002) 4.657, 100, (200) 3.365, 55, ($\bar{3}$02)	8.86, 85, (100) 4.438, 100, ($\bar{1}$11) 3.383, 60, (102) 2.833, 50, ($\bar{3}$12)
d, I, (hkl)	3.071, 54, (1$\bar{1}$2) 2.735, 48, ($\bar{3}$1$\bar{2}$)	2.818, 45, (112) 2.222, 30, (400)
Optics	Biaxial (–) $\alpha = 1.642(2)$, $\beta = 1.659$ (calc), $\gamma = 1.660(2)$ 2V(meas) = 27(1)°	Biaxial (–) $\alpha = 1.595$, $\beta = 1.614$, $\gamma = 1.616$ 2V(calc) = 44.3°

connectivities for the two minerals shown in Fig. 7, which results in a 5% expansion of the interlayer spacing in steinmetzite. The powder XRD patterns for the two minerals are quite different as illustrated by Fig. 1. The Fe^{3+}-containing steinmetzite also has considerably higher (by ~3%) refractive indices than the Fe^{2+}-containing phosphophyllite.

Acknowledgements

The authors thank Peter Leverett, Nikita Chukanov, an anonymous reviewer and the Associate Editor Andrew Christy who provided helpful comments to improve the manuscript.

References

Birch, W.D., Grey, I.E., Mills, S.J., Pring, A. Wilson, N.C. and Keck, E. (2011) Nordgauite, $MnAl_2(PO_4)_2(F,OH)_2\cdot 5.5H_2O$, a new mineral from the Hagendorf Süd pegmatite, Bavaria, Germany: description and crystal structure. *Mineralogical Magazine*, **75**, 269–278.

Forster, A., Strunz, H. and Tennyson, Ch. (1967) Die Pegmatite des Oberpfälzer Waldes insbesondere der Pegmatit von Hagendorf Sud. Pp. 137–198 in: *Zur Mineralogie und Geologie der Oberpfalz* (R. Metz, editor). Heidelberg, Germany [Der Aufschluss Sonderheft 16].

Grey, I.E., Keck, E., Kampf, A.R., Mumme, W.G., MacRae, C.M., Gable, R.W., Glenn, A.M. and Davidson, C.J. (2015*a*) Steinmetzite, IMA 2015-081. CNMNC Newsletter No. 28, December 2015, page 1863*; Mineralogical Magazine*, **79**, 1859–1864.

Grey, I.E., Keck, E., Mumme, W.G., Pring, A., MacRae, C.M., Gable, R.W. and Price, J.R. (2015*b*) Flurlite, $Zn_3Mn^{2+}Fe^{3+}(PO_4)_3(OH)_2\cdot 9H_2O$, a new mineral from the Hagendorf Süd pegmatite, Bavaria, with a schoonerite-related structure. *Mineralogical Magazine*, **79**, 1177–1186.

Grey, I.E., Keck, E., Mumme, W.G., Pring, A., MacRae, C.M., Glenn, A.M., Davidson, C.J., Shanks, F.L. and Mills, S.J. (2016) Kummerite, $Mn^{2+}Fe^{3+}Al(PO_4)_2(OH)_2\cdot 8H_2O$, a new laueite-group mineral from the Hagendorf Süd pegmatite, Bavaria, with ordering of Al and Fe^{3+}. *Mineralogical Magazine*, **79**, 1243–1254.

Grey, I.E., Keck, E., Kampf, A.R., MacRae, C.M., Glenn, A.M. and Price, J.R. (2017) Wilhelmgümbelite, $[ZnFe^{2+}Fe_3^{3+}(PO_4)_3(OH)_4(H_2O)_5]\cdot 2H_2O$ a new schoonerite-related mineral from the Hagendorf Süd pegmatite, Bavaria. *Mineralogical Magazine,* **81,** 287–296.

Gunter, M.E., Bandli, B.R., Bloss, F.D., Evans, S.H., Su, S.C. and Weaver, R. (2004) Results from a McCrone spindle stage short course, a new version of EXCALIBR, and how to build a spindle stage. *The Microscope*, **52**, 23–39.

Hawthorne, F.C. (1988) Sigloite: The oxidation mechanism in $[M_2^{3+}(PO_4)_2(OH)_2(H_2O)_2]^{2-}$ structures. *Mineralogy and Petrology*, **38**, 201–211.

Hill, R.J. (1977) The crystal structure of phosphophyllite. *American Mineralogist*, **62**, 812–817.

Laubmann, H. and Steinmetz, H. (1920) Phosphatführende Pegmatite des Oberfalzer und Bayerischen Waldes. *Zeitschrift für Kristallographie*, **55**, 523–586.

Mandarino, J.A. (1981) The Gladstone-Dale relationship: Part IV. The compatibility concept and its application. *The Canadian Mineralogist*, **19**, 441–450.

Mills, S.J. and Grey, I.E. (2015) Nomenclature for the laueite supergroup. *Mineralogical Magazine*, **79**, 243–246.

Mills, S.J., Grey, I.E., Kampf, A.R., Birch, W.D., MacRae, C.M., Smith, J.B. and Keck, E. (2016) Kayrobertsonite, $MnAl_2(PO_4)_2(OH)_2 \cdot 6H_2O$, a new phosphate mineral related to nordgauite. *European Journal of Mineralogy*, **28**, 649–654.

Mücke, A. (1981) The paragenesis of the phosphate minerals of the Hagendorf pegmatite – a general view. *Chemie der Erde*, **40**, 217–234.

Petříček, V., Dušek, M. and Palatinus, L. (2014) Crystallographic Computing System JANA2006: General features. *Zeitschrift für Kristallographie – Crystalline Materials*, **229**, 345–352.

Rodriguez-Carvajal, J. (1990) *FULLPROF: A Program for Rietveld Refinement and Pattern Matching Analysis*. Satellite meeting on powder diffraction of the XV Congress of the IUCr, Toulouse, France.

Steinmetz, H. (1926) Phosphophyllit und Reddingit von Hagendorf. *Zeitschrift für Kristallographie*, **64**, 405–412.

Yakovenchuk, V.N., Keck, E., Krivovichev, S.V., Pakhomovsky, Y.A., Selivanova, E.A., Mikhailova, J.A., Chernyatieva, A.P. and Ivanyuk, G.Yu. (2012) Whiteite-(CaMnMn), $CaMnMn_2Al_2[PO_4]_4(OH)_2 \cdot 8H_2O$, a new mineral from the Hagendorf-Süd granitic pegmatite, Germany. *Mineralogical Magazine*, **76**, 2761–2771.